DEFENS INFORM Buildin Alexar

AD-A256 668

Form Approved
OMB No 0704-0188

Public reporting burden including the time for reviewing instructions, searching existing data sources, gathering and maintaining the data needed, and completing and reviewing the collection of information. Send comments regarding this burden estimate or any other aspect of this collection of information, including suggestions for reducing this burden, to Washington Headquarters Services, Directorate for information Operations and Reports, 1215 Jefferson Davis Highway, Suite 1204, Arlington, VA 22202-4302, and to the Office of Management and Budget, Paperwork Reduction Project (0704-0188), Washington, DC 20503.

1. AGE	2. REPORT DATE	3. REPORT TYPE AND DATES COVERED
(Leave blank)	25 August 92	Reprint

4. TITLE AND SUBTITLE

Comparing Model-produced Convective Cloudiness with Observations

5. FUNDING NUMBERS

PE 62101F
PR 6670
TA 10
WU 28

6. AUTHOR(S)

D.C. Norquist, C. Yang

7. PERFORMING ORGANIZATION NAME(S) AND ADDRESS(ES)

Phillips Lab/GPAP
Hanscom AFB
Massachusetts 01731-5000

DTIC ELECTE SEP 03 1992 S B D

8. PERFORMING ORGANIZATION REPORT NUMBER

PL-TR-92-2220

9. SPONSORING/MONITORING AGENCY NAME(S) AND ADDRESS(ES)

10. SPONSORING/MONITORING AGENCY REPORT NUMBER

11. SUPPLEMENTARY NOTES

Reprinted from Monthly Weather Review, Vol 120, No. 5 May 1992
American Meteorological Society

12a. DISTRIBUTION/AVAILABILITY STATEMENT

Approved for public release; Distribution unlimited

12b. DISTRIBUTION CODE

13. ABSTRACT (Maximum 200 words)

Convective cloudiness generated by a cumulus parameterization scheme of a large-scale numerical weather prediction model was compared with analyses of clouds observed by geosynchronous satellites. The comparisons were performed over an equatorial Pacific Ocean region and the Amazon basin region for the period January–February 1979. Fractional coverage of predefined areas by clouds with tops in several altitude-temperature categories was averaged in each area for the entire period of record and also for individual times of the day. The overall mean provided a basis for comparison of the general spatial distributions of observed and model-produced cloud, while hourly departures from the overall mean allowed a comparison of the diurnal variations.

Geosynchronous satellite cloud analysis serves as a useful reference for assessing the performance of a moist convective parameterization scheme. In this case, it was found that the subject convective scheme produces an accurate relative horizontal distribution of convective cloudiness, but produces too large a proportion of deep convection compared to overall convection. This was believed to be due to a lack of an entrainment mechanism in the scheme. The diurnal variation of model-produced convection was 9–12 h out of phase and somewhat smaller in magnitude than the observed variation over the ocean region. Good agreement was noted between the diurnal characteristics of observed cloud and model-produced convection over the land region.

14. SUBJECT TERMS

Number weather prediction, Satellite observations of clouds, Cloud forecasting

15. NUMBER OF PAGES

17

16. PRICE CODE

17. SECURITY CLASSIFICATION OF REPORT	18. SECURITY CLASSIFICATION OF THIS PAGE	19. SECURITY CLASSIFICATION OF ABSTRACT	20. LIMITATION OF ABSTRACT
Unclassified	Unclassified	Unclassified	SAR

PL-TR-92-2220

Reprinted from MONTHLY WEATHER REVIEW, Vol. 120, No. 5, May 1992
American Meteorological Society

Comparing Model-produced Convective Cloudiness with Observations

D. C. NORQUIST AND C. YANG

92 9 01 008

92-24208

Comparing Model-produced Convective Cloudiness with Observations

D. C. NORQUIST AND C. YANG

Atmospheric Sciences Division, Geophysics Directorate, Phillips Laboratory (AFSC), Hanscom AFB, Massachusetts

(Manuscript received 25 January 1991, in final form 10 June 1991)

ABSTRACT

Convective cloudiness generated by a cumulus parameterization scheme of a large-scale numerical weather prediction model was compared with analyses of clouds observed by geosynchronous satellites. The comparisons were performed over an equatorial Pacific Ocean region and the Amazon basin region for the period January–February 1979. Fractional coverage of predefined areas by clouds with tops in several altitude–temperature categories was averaged in each area for the entire period of record and also for individual times of the day. The overall mean provided a basis for comparison of the general spatial distributions of observed and model-produced cloud, while hourly departures from the overall mean allowed a comparison of the diurnal variations.

Geosynchronous satellite cloud analysis serves as a useful reference for assessing the performance of a moist convective parameterization scheme. In this case, it was found that the subject convective scheme produces an accurate relative horizontal distribution of convective cloudiness, but produces too large a proportion of deep convection compared to overall convection. This was believed to be due to a lack of an entrainment mechanism in the scheme. The diurnal variation of model-produced convection was 9–12 h out of phase and somewhat smaller in magnitude than the observed variation over the ocean region. Good agreement was noted between the diurnal characteristics of observed cloud and model-produced convection over the land region.

1. Introduction

Cumulus parameterization schemes in large-scale models are difficult to verify. Such schemes produce heating and moistening profiles that modify the large-scale environment. Since direct measurements of cumulus heating and moistening are not available, researchers such as Yanai et al. (1973), Miller and Vincent (1987), and others have deduced heating and moistening profiles from conventional observations. These studies have involved the computation of heating sources and moisture sinks as a residual from the classic heat and moisture budget equations. These estimates are only as good as the estimate of the magnitudes of the other terms (such as boundary-layer fluxes and net radiation), which are based on either uncertain observations or another model.

Studies such as those by Lord (1982) and Grell et al. (1988) have used "observed" heating profiles deduced from experimental datasets to verify semiprognostic tests of their cumulus heating parameterizations. Besides the aforementioned uncertainty of the reference heating profile, such studies are hampered by the inability to examine the realism of the scheme's performance in a model integration exercise. Infrequent conventional observations permit only a diagnosis of a single "snapshot" of the model atmosphere and not the statistical analysis of a series of model integrations. On the other hand, the fact that the semiprognostic approach does not march in time is seen as an advantage because it is free from model error sources other than those of the cumulus parameterization. Still, such studies rely on datasets taken from experimental field programs limited to a few regions of the globe and times of the year.

Convective cloudiness as observed by geostationary satellites offers a data source nearly continuous in time and space that may be exploited to evaluate a cumulus parameterization scheme's performance for an ensemble of forecasts. In particular, infrared satellite cloud-top brightness temperatures can be used to determine the approximate altitude or pressure level of the cloud top assuming a knowledge of the vertical temperature structure. Infrared cloud imagery can thus be used to estimate fractional cloud coverage over an area as a function of cloud-top altitude or temperature.

Similarly, cloudiness produced by a cumulus parameterization can be diagnosed over an ensemble of forecasts corresponding to the time and space sample analyzed from satellite data. Then a direct comparison can be made of fractional cumulus coverage between like ensembles of observed and model-produced cumulus. Comparison for hourly departures from the daily mean for both observed and model-produced cumulus allows an assessment of the model's diurnal cycle. The purpose of this paper is to show how the per-

Corresponding author address: Donald C. Norquist, Department of the Air Force, PL/GPAP, Hanscom Air Force Base, MA 01731-5000.

formance of a cumulus parameterization scheme within a large-scale model may be evaluated against satellite-observed cloudiness.

Albright et al. (1985) reduced GOES-West infrared satellite data over a limited region of the equatorial Pacific Ocean to produce estimates of fractional cloud cover within 1.5° lat–long squares. This was done for cloud tops within certain temperature ranges for the period 13 January–5 February 1979. They computed the overall time period average of fractional cloudiness in each square for each range of cloud-top temperatures (tops cooler than −18°, −36°, and −55°C). These averages were based on data available at 3-h intervals. They then computed the same averages at each 3-h UTC time and subtracted the overall average from each 3-h average to compute the departures from the daily mean at each 3-h UTC time.

Minnis and Harrison (1983) performed a similar study using GOES-East data over a limited region that included the Amazon basin. They generated total, low-, middle-, and high-cloud fractional coverages within 250 × 250-km^2 squares for the period 30 January–15 February 1979. Cloud-top height categories were defined as: low clouds—altitudes less than 2 km; middle clouds—altitudes between 2 and 6 km; and high clouds—altitudes greater than 6 km. The 24-h average clear-sky infrared surface temperature and a 6.5 K km^{-1} lapse rate were used to assign cloud-top temperatures to the proper altitude category. Minnis and Harrison (1983) computed local time hourly averages for each square. They then identified the local hour with the maximum and minimum cloudiness for each square. The difference between the maximum and minimum fractional cloudiness they termed the *diurnal range*.

A knowledge of the fractional coverage by actual cloud tops indicative of shallow, moderate, and deep convection provides information useful in determining the veracity of model performance. A cumulus parameterization scheme should replicate the time-averaged observed vertical extent of cloudiness. The scheme may consistently produce deep convection where only shallow or moderate convection is typically observed to exist. In this case, we would conclude that the scheme has a systematic error. The simulation of latent heat release at upper levels where in fact no convection occurs has important implications on the large-scale forecasts produced by the model. Such a discrepancy in the temporal distribution would also be important in daily forecasts of cloudiness. By comparing the diurnal pattern of observed and model-produced convective cloudiness, one can determine the realism of the model's simulation of the diurnal cycle of convection.

It is recognized that not all of the cloudiness observed by infrared satellite sensors is convective. There is sure to be cloudiness data analyzed in these studies that are not of cumuliform. This is particularly true of low-cloud observations made in the Amazon basin. It is also true that cirrus anvils often accompany deep convection. The spatial coverage of the cloud top, including the anvil, represents a greater area as viewed by the satellite than the area covered by cumuliform cloud simulated by the model. Thus, in areas of observed deep convection, it may be expected that the satellite would report a greater coverage of cloud than would be simulated by the model. Furthermore, Leary and Houze (1980) observed that anvils can outlast the cumulus that produce them; therefore, it is possible that time lags can exist between peak cumulus activity and satellite-observed cloudiness.

Cumulus is the dominant cloud type in convectively active regions of the tropics, especially in the middle and high (or colder than −36° and −55°C) categories. Nevertheless, since the presence of other cloud types is an undeniable reality in cloud observations by satellites, it is difficult to sort out just the cumulus. The assumption that total cloudiness increases with convective cloudiness is made (especially for middle and high cloud) so that a relative comparison with model-generated cumulus is possible. That is, spatial and temporal distributions of cloudiness can be qualitatively compared only within the vertical range categories, assuming that cumuliform cloud is the dominant observed cloud type. A quantitative comparison of the amount of cloudiness is outside the scope of this study.

The nature of the parameterization problem brings yet another complication to the comparison of model-produced cumulus with observations in the case of bulk (single cloud type) schemes. Because the parameterization scheme simulates the effect of cumulus convection on the large-scale environment, the scheme produces a uniform cumulus representation at a grid point per model time step. By contrast, the cloud coverage in the infrared satellite data can vary by cloud-top temperature within analysis grid square. Several individual cloud elements, each with its own distinct cloud-top temperature, may exist simultaneously in the grid square. Thus, even at a given time, the observation may have a range of cumulus depths within a grid square. The bulk model can only produce such a range over one or more numerical forecasts. Therefore, one must have a time sample of model integrations and satellite observations for a valid comparison of average cloud cover as a function of cloud altitude at a grid point.

Finally, the mutual dependence between the convective scheme and the rest of the large-scale model is noted. Feedbacks occur between the various model components such that a given convective scheme may perform quite differently in a different large-scale model. Thus, the approach of this study can only be used to validate the cumulus scheme within the context of the parent model.

In this paper, the convective cloudiness generated by a cumulus parameterization scheme of a large-scale model is compared with the analysis of cloud observations performed by Albright et al. (1985) and Minnis and Harrison (1983). The following section describes the forecast data and how they were processed to facilitate these comparisons. Section 3 discusses results of the comparisons, and section 4 summarizes the conclusions.

2. Data and methods

An early version of the Phillips Laboratory (PL) global spectral model (GSM) has been described and used in data assimilation experiments by Louis et al. (1989). The 30-wave rhomboidal truncation requires a transform grid of 76 Gaussian latitude points and 96 regularly spaced longitude points for a computation of the nonlinear processes within the model. Thus, each grid box represents an area of approximately 2.35° latitude and 3.75° longitude.

The current version of PL GSM differs from the earlier version in two major respects. First, the vertical resolution has been increased from 12 to 18 sigma (pressure/surface pressure) layers. The sigma layer interfaces are at 0.000, 0.050, 0.100, 0.150, 0.200, 0.250, 0.300, 0.350, 0.400, 0.450, 0.546, 0.642, 0.735, 0.820, 0.893, 0.948, 0.973, 0.990, and 1.000. This vertical structure is the same as that of the National Meteorological Center (NMC) Medium-Range Forecast (MRF) Model (Kanamitsu 1989). The second major modification has been the replacement and addition of the physics model. Mahrt et al. (1987) developed a planetary boundary-layer parameterization that is applied over both land and ocean surfaces. Liou et al. (1984) designed a scheme that calculates both infrared and solar radiation transfers in both clear and cloudy atmospheres. Krishnamurti et al. (1976) proposed a closure for the Kuo (1974) cumulus parameterization scheme that allows the computation of the moisture partitioning parameter. Also, evaporation of falling precipitation within the cloudy portion of the grid box, a new computation of the lifting condensation level and moist adiabat, and a center-difference (in time) moisture convergence computation were added (Norquist and Yang 1990). All three parameterization packages were used in the PL GSM.

The PL GSM was initialized using the reanalyzed FGGE III analyses for 1200 UTC on the following dates: 12, 16, 20, 24, 28 January and 1, 5, 9 February 1979. These dates were chosen to coincide with the analyses of cloud data from geosynchronous satellites by Albright et al. (1985) and Minnis and Harrison (1983). The model-generated cumulus in this study was compared directly with their results.

Five-day forecasts were produced from each of the aforementioned initial dates. To avoid the classic convective spinup deficiency in the initial hours of each forecast run, only forecasts for hours 25–120 of each period were included in the overall forecast sample. For the grid points lying within the regions of interest, the precipitation rate, cloud-top temperature, and (for the Amazon basin region) lowest model-layer temperature were extracted. Cloud-top temperature was determined by a linear interpolation in the natural logarithm of pressure to the pressure level where the moist adiabat temperature equals the environmental temperature (level of zero buoyancy in a nonentraining cloud).

Another quantity that was calculated within the convective parameterization scheme is the fractional coverage of the grid box by convective cloud (Kuo 1974). This fraction accounts only for the cumulus cylinder, not for any horizontal spreading of the cumulus as it develops vertically, nor for the cirrus outflow. For this reason, an empirical relationship between observed tropical convective cloudiness and model-produced precipitation was sought that would yield a realistic depiction of convective cloudiness from the model's convective rainfall rates. Several studies, including Albright et al. (1985) and Arkin and Meisner (1987), have cited such empirical relationships based on observations of precipitation rates and satellite brightness temperatures. Slingo (1987) cites an empirical relationship derived from a comparison of model precipitation rates and frequency distributions of tropical convective cloudiness. Slingo states that the scheme has been used successfully to diagnose convective cloud amounts with two different convective parameterizations (including Kuo) in the context of a large-scale model. Because of the need to relate model-produced precipitation to satellite-observed convective cloudiness in the tropics, Slingo's (1987) formula was used to compute fractional coverage of a grid square by convective cloud C_c from model precipitation rate P in millimeters per day. That formula is $C_c = a + b \ln P$, in which the empirical constants $a = 0.24733$ and $b = 0.12580$ were derived from Table 1 of Slingo (1987) (which gives discrete values of C_c and corresponding P). The value of C_c was constrained to a value not to exceed 0.8. Slingo's areal reduction factor for deep convection (only 25% of the predicted amount allowed to occupy the full depth) was not used for two reasons. First, Slingo states that it is an assumption (not necessarily based on quantitative empirical evidence) made to represent the relatively small fraction of the sky occupied by cumulonimbus compared to lower-level convection. Second, all model convection considered in this study exceeds Slingo's criterion for deep convection (extending above 400 mb). Therefore, the relative cloud amounts would remain the same for all cloud-top temperature categories.

In the equatorial Pacific region, the instantaneous precipitation rate was used at the 3 h centered around

0000, 0300, 0600, 0900, 1200, 1500, 1800, and 2100 UTC to compute a 3-h average value at each of these eight times. The averaging formula gave a weight of 0.25 to the value at the hour before and after the central time, and a weight of 0.50 to the central time value. The fractional cloud amount C_c for each of the eight UTC times was computed from the averaged precipitation rate. The coldest of the three cloud-top temperatures was assigned to represent the cloud's 3-h value. This dictated the cloud-top temperature category (colder than −18°, −36°, or −55°C) in which to place the cloud. If cloud-top temperature was not cold enough to include the cloud in a particular temperature category, zero cloud was attributed to that category for that time period. Then the computed fractional cloud amounts were averaged by cloud-top temperature category for each UTC time and over all eight UTC times for each model grid box. The six 4-day forecast periods resulted in an overall time sample covering the period 1200 UTC 13 January 1979 to 0900 UTC 6 February 1979. This period coincides closely with the period of cloud analysis performed by Albright et al. (1985).

In the Amazon basin region, following Minnis and Harrison's (1983) example, averages of model fractional cloud amount were computed for each hour of local time at each model grid box. The hourly grid-box cloud amount was derived directly from the hourly precipitation rate. In addition, an overall time average of fractional cloud amount was computed at each grid box. This was done for total cloud (that is, the diagnosed cloud amount without regard to cloud-altitude category) and for individual altitude categories. The reference temperature for a given altitude was determined from the lowest model-layer temperature and assuming a 6.5°C km^{-1} lapse rate. The cloud-top temperature was compared with the reference temperature to place the cloud top in one of the three altitude categories of Minnis and Harrison (1983): low (less than 2 km), middle (between 2 and 6 km), or high (greater than 6 km). Unlike the equatorial Pacific region study where cloud may exist in as many as three altitude categories, cloud was assigned to the total category and only one of the altitude categories. Thus, value of zero cloud is registered in the computation of the average of the other two altitude categories for that local time.

As was done by Minnis and Harrison (1983), the overall time-average fractional cloud amounts in each of the cloud altitude categories were expressed as a percentage of the overall time average of total cloud for each grid box. Then for each grid box, the local times with the maximum and minimum average cloud fraction for each altitude category were identified. The maximum–minimum difference represents the diurnal range for each category. Four 5-day model runs generating forecasts covering the period 1300 UTC 29 January–1200 UTC 14 February 1979 contributed data to the forecast sample. The period coincides with the period of satellite observations of cloudiness analyzed by Minnis and Harrison (1983).

3. Results

a. Equatorial Pacific region

The sample average model-generated cumulus coverages for the equatorial Pacific region are shown in Fig. 1 for each cloud-top temperature category. The corresponding satellite-observed averages are reproduced here as Fig. 2 from Fig. 5 of Albright et al. (1985). In both cases, the threshold temperatures of −18°, −36°, and −55°C delineate the vertical extent of the cumulus penetration. These temperatures correspond approximately to pressure levels of 40, 28, and 20 kPa, respectively. Longitudes in Fig. 1 are expressed in east longitude; the right side of each plot corresponds to 127.5°W. The center of both sets of figures lies at 160°W (200°E). Figure 1 has a slightly greater extent in longitude than Fig. 2 in order to accommodate enough model grid points to cover the longitude domain of 170°E–130°W in Fig. 2.

The zone of maximum cloudiness in Fig. 2a (values greater than 30%) marks the location of the South Pacific convergence zone (SPCZ). This zone is reflected in maximum cloudiness values in Figs. 2b and 2c as well. The presence of this maximum in all three figures indicates that this zone is characterized by some deep convection; however, the fractional cloudiness is reduced significantly with altitude, indicating that only a small portion of the convection penetrates above −55°C. The axis of the SPCZ as indicated by Fig. 2a is an arc from 5° to 7°S at the western edge of the area, down to 148°W at 17°S, the southern edge.

A zone of maximum cloudiness (here, greater than 25%) is apparent in the model-generated clouds as seen in Fig. 1a. The axis of this zone arcs from 10°S at 168.75°E to approximately 206°E (154°W) at 15°S. The similarity between averages for the −18° and −36°C categories indicates that virtually all of the model-generated convection reaching −18° also penetrates to −36°C. In fact, in the western portion of the zone of maximum cloud coverage, most of the convection that reaches −18° also ascends to −55°C (see Fig. 1c).

A zone of secondary maximum cloudiness centered on 10°N in the eastern half of the region is evident in Figs. 1a and 1b. Values of average cloud cover greater than 25% are also evident in this zone in both −18° and −36°C categories; however, compared to the SPCZ, this area has a more distinct reduction of cloud coverage between −18° and −36°C. In addition, very few (less than 5% coverage) of the model-produced cumulus have tops colder than −55°C in this area. According to Albright et al. (1985), this axis of secondary maxima corresponds to the intertropical convergence

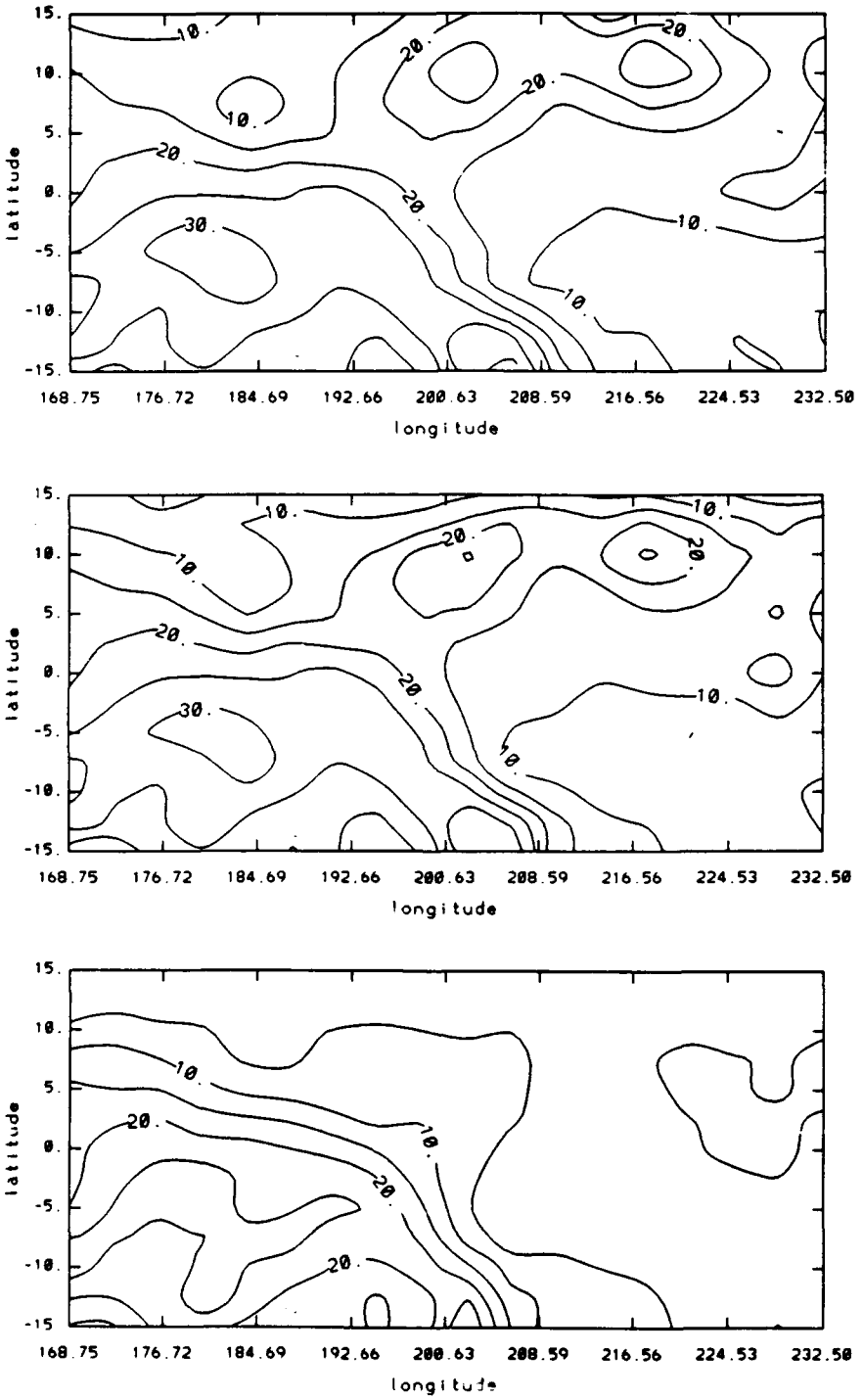

FIG. 1. Average model-generated percent cumulus coverage during the period 13 January–6 February 1979 for model grid boxes (2.35° lat × 3.75° long) by clouds with tops colder than (a) −18°C, (b) −36°C, (c) −55°C.

zone (ITCZ) (see their Fig. 2). A similar (but weaker) zone of cloudiness is evident in the satellite-observed clouds in Fig. 2a, b.

The percent departure from daily average of model-generated cumulus cloud coverage for cloud tops colder than −36°C is shown in Figs. 3a–h for 3-h intervals

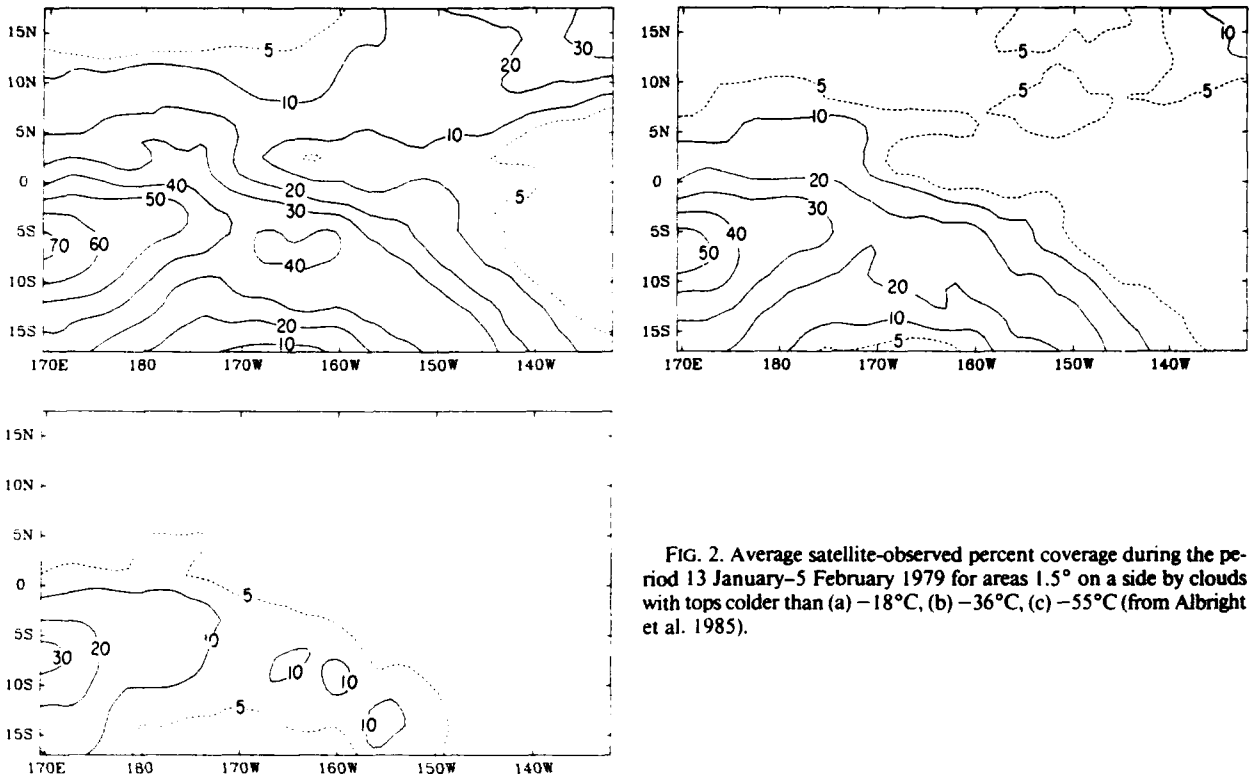

FIG. 2. Average satellite-observed percent coverage during the period 13 January–5 February 1979 for areas 1.5° on a side by clouds with tops colder than (a) −18°C, (b) −36°C, (c) −55°C (from Albright et al. 1985).

from 0000 to 2100 UTC. Corresponding plots for the −18° and −55°C thresholds (not shown) exhibit spatial patterns similar to those of the −36°C figures shown. This was particularly true for the −18°C threshold. Maxima and minima of approximately the same size and magnitude were evident. In the case of the −55°C plot, departures were present only in the SPCZ and were of somewhat lesser magnitude than for −36°C. This reflects the relationship between the period average plots shown in Figs. 1b and 1c. Most of the model-produced convection attains all three threshold temperature levels in the SPCZ only.

In Fig. 3, we see the areas of largest departure from the average of convective cloudiness occur in the SPCZ at local midnight (see Fig. 3e). Three hours later (Fig. 3f) these areas are somewhat reduced in areal extent and magnitude and are displaced to the north. In the early morning hours (Fig. 3g) the maxima have increased from 3 h earlier and are still farther to the north, now more coincident with the ITCZ. By 0900–1000 LST (Fig. 3h) the maxima have stabilized their position, and only the eastern maximum has retained its value.

It is at this time that the minima take over in the area of the SPCZ. Large areas of minima as high as −9% (more than 25% of the mean) are evident at both 0900 (Fig. 3-h) and 1200 LST (Fig. 3a). The negative departures diminish in magnitude but are still evident in the SPCZ at 1500–1600 (Fig. 3b), and by 1800 LST (Fig. 3c) have given way to the growth of positive departures. These positive departures grow in intensity and area until their maxima are reached at local midnight.

Looking back at Fig. 1b, recall that the secondary maximum areas of cloudiness corresponding to the ITCZ were present at 10°N in the eastern half of the region. In tracing the diurnal cycle of this band of cloudiness, we find from Fig. 3 that no clear diurnal pattern is evident. There is some suggestion of positive departures in the vicinity at 1300–1400 (Fig. 3a) and 1600–1700 LST (Fig. 3b) and negative departures at 2300 (Fig. 3d) and 1100 LST (Fig. 3h); however, the amplitude of these departures is smaller, and the peaks are less distinct in time than in the SPCZ area.

Figure 7 of Albright et al. (1985) has been reproduced as Fig. 4 to allow a visual comparison with Fig. 3. The observed cloudiness in the SPCZ achieves its maximum values in the afternoon (1300–1700 LST) as is evident from Figs. 4a and 4b. While some cloudiness maxima are still apparent in the extreme southwestern portion of the region between 1700 and 2000 LST, the central and eastern portions of the SPCZ experience cloudiness minima between 1800 and 0100 LST. The plots of diurnal variation of the observed cloudiness for −18°C in Albright et al. (1985) show a rather clear maximum in the ITCZ between 0000 and 0300 LST and a minimum between 1100 and 1500 LST. These areas do

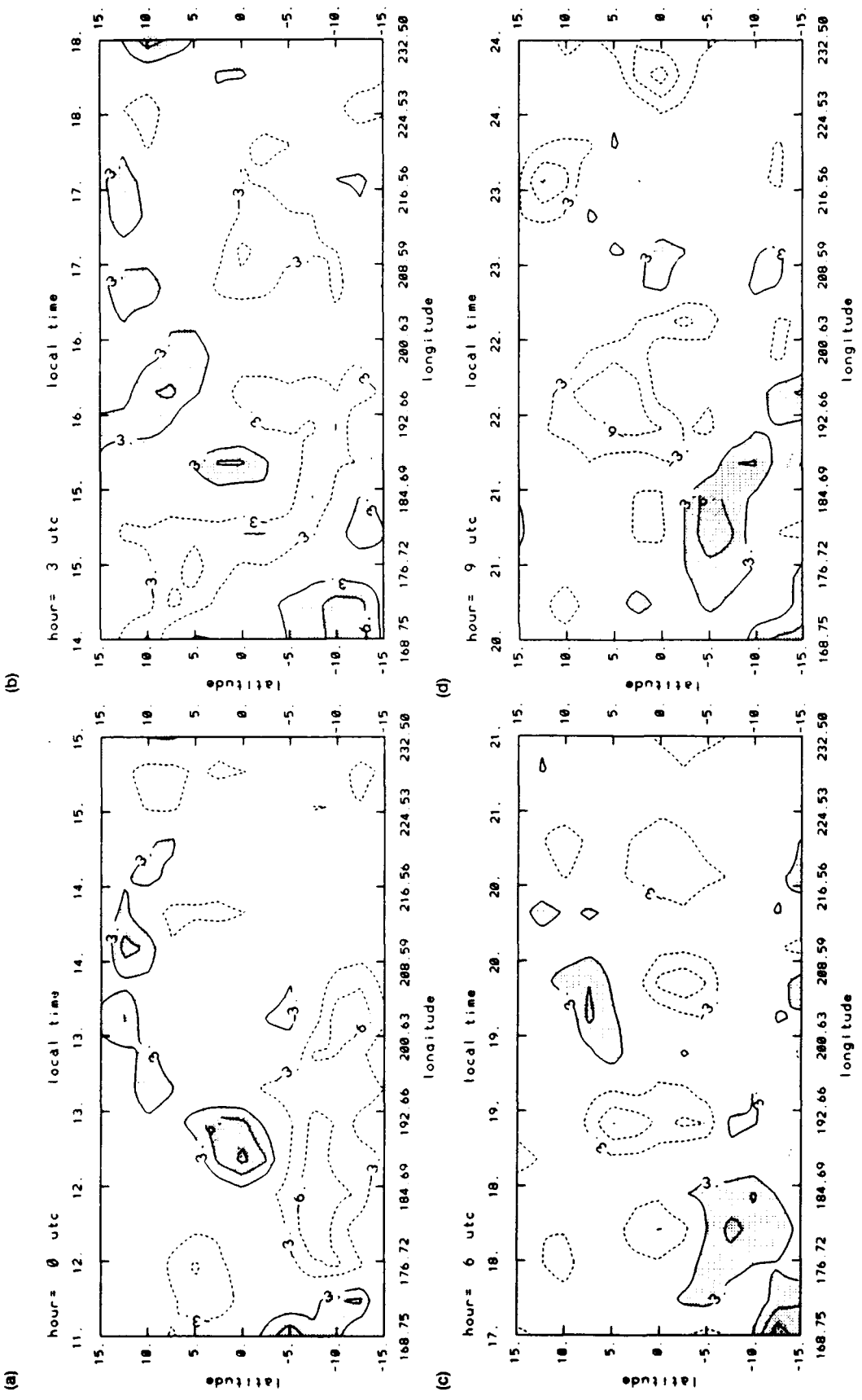

FIG. 3. Diurnal variation of the percent coverage by model-generated cumulus with tops colder than −36°C, expressed as departures from the average percent coverage.

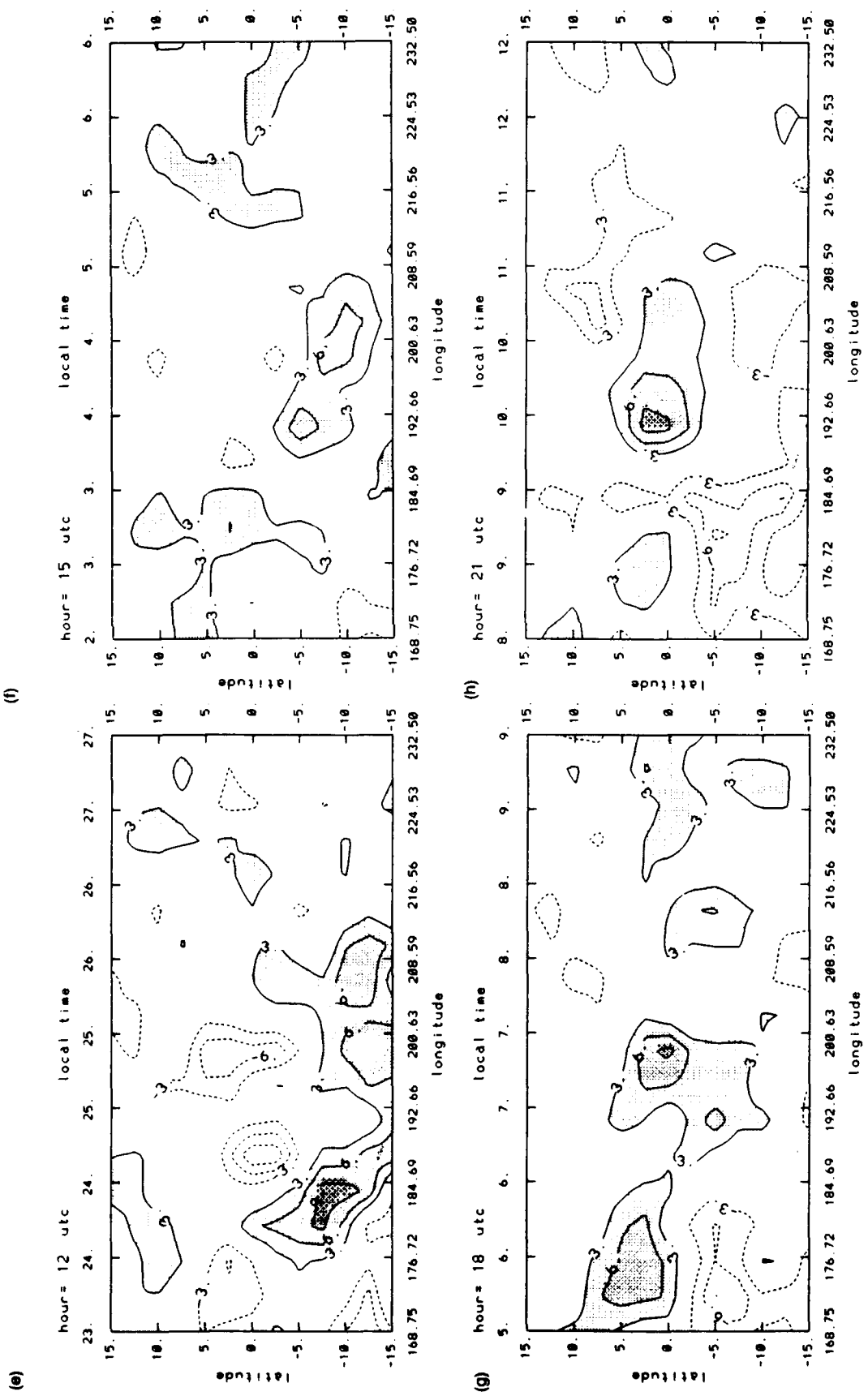

FIG. 3. (*Continued*)

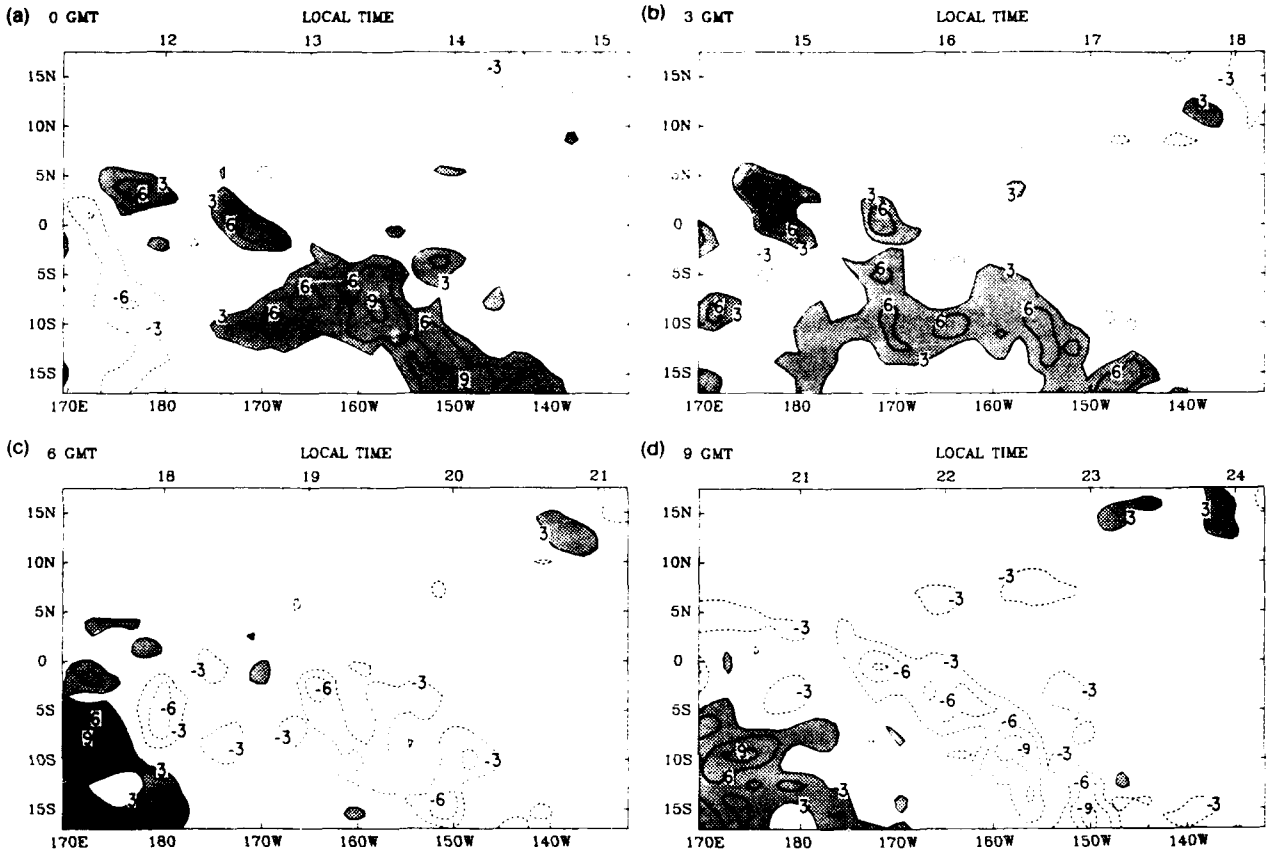

FIG. 4. Diurnal variation of the percent coverage by satellite-observed cumulus with tops colder than −36°C, expressed as departures from the average percent coverage (from Albright et al. 1985).

not appear in Fig. 4 because of the relatively shallow nature of the observed convection in the northeastern portion of the region (compare Figs. 2a and 2b).

b. Amazon basin region

Average total cloud cover from the 29 January–14 February 1979 forecasts for the Amazon basin region are shown in Fig. 5. The largest total cloud coverage values are located over the southern Amazon basin. The zone of greatest total cloud cover is located along an axis oriented from northwest to southeast. A smaller area of maximum cloud cover lies southwest of the major area. Both of these areas contain values exceeding 50% total cloud coverage, which is considerably greater than the maximum values exceeding 30% coverage for the equatorial Pacific region.

Average high-cloud coverage is shown as a percentage of total cloud coverage for model-generated cumulus in Fig. 6. Almost all of the total cloud coverage over the Amazon basin and central South America is due to high (tops higher than 6 km) cloud. Because virtually all of the model-generated cumulus penetrates to levels above 6 km, it was unnecessary to show the low- and middle-cloud coverage plots. To put this altitude in perspective, the equivalent standard tropical atmosphere temperature and pressure at 6 km are approximately −10°C and 49 kPa (*U. S. Standard Atmosphere Supplements* 1966). Thus, nearly all model-produced convection exceeds midtropospheric levels over continental South America during its season of greatest convective activity.

Figure 7 depicts the average total cloud cover for the period 30 January–15 February 1979 as analyzed from GOES satellite data by Minnis and Harrison (1983). Values as high as 90%–100% average cloud cover are in evidence over the central Amazon basin. Cloud coverage greater than 70% (the red area) covers essentially all of the Amazon basin and spreads southeastward into the southern Atlantic Ocean.

Maps of outgoing longwave radiation (OLR) prepared by Bess and Smith (1987) for January and February 1979 show minima of OLR centered over this same area. They depict satellite-observed average OLR of less than 200 W m^{-2} over the central Amazon basin and values of less than 230 W m^{-2} extending over the southern Atlantic Ocean. These low values of OLR are characteristic of radiation emitted from the tops of

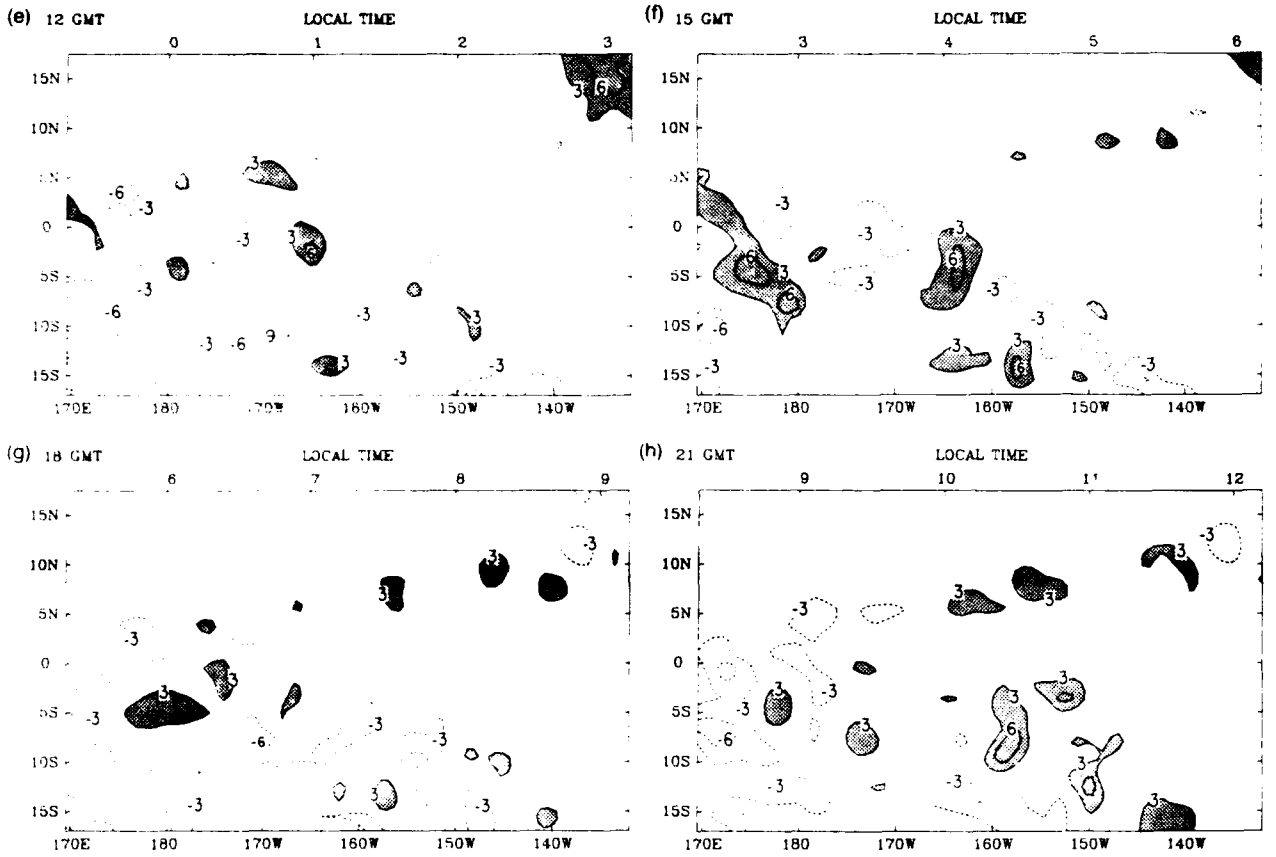

FIG. 4. (*Continued*)

moderate-to-deep cumulus clouds. They have an emitting temperature lower than warmer surfaces such as low clouds or the earth's surface.

Some 30%–40% of the observed total cloud cover over the central and eastern Amazon basin is made up of high cloud, according to Fig. 8. Observed middle-cloud cover was in the range of 40%–50% of the total over almost the entire area of total cloudiness exceeding 70%. Only on the southeastern Brazilian coastline and just offshore does observed high-cloud cover exceed that of middle-cloud cover.

The diurnal range (difference between maximum and minimum hourly averages) of model-generated high cloud cover is shown in Fig. 9. In the interior of the Amazon basin, values exceeding 30% are in the majority. Recalling that high cloud made up almost all of the total cloud cover depicted in Fig. 5, we can see by comparing Fig. 9 with Fig. 5 that the amplitude of cloud-cover maxima (half the diurnal range) is commonly 50%–100% of the mean. Thus, the model-produced diurnal variation is much greater in amplitude over the Amazon basin than over the equatorial Pacific. The maximum total cloud cover for model-generated cumulus (Fig. 10) occurs in the afternoon hours (1200–1700 LST) throughout most of the Amazon basin.

The diurnal range of observed high cloudiness from the Minnis and Harrison (1983) study is depicted in Fig. 11. Over the Amazon basin, virtually all of the area is characterized by 30%–50% maximum-to-minimum ranges. Since observed high cloud made up some 40% of the total cloud cover (observed to be at least 70% coverage over the region), it can be said that the mean high-cloud coverage was at least 28% (0.4 of the 70% total coverage). This means that the amplitude of the diurnal variation of cloud cover of the observed high clouds was 50%–90% of the mean. The time of maximum total cloud cover for observed clouds in the western portion of the Amazon basin was 0000–0600 LST, and for the eastern portion, generally 0800–1200 LST. However, according to Minnis and Harrison (1983), the time of day for maximum high-cloud cover (indicating primarily convective cloud) appears to occur in the late afternoon (1500–1800 LST) over most of the Amazon basin (see their Fig. 10).

4. Conclusions

In this paper we have evaluated the cloud production of a typical large-scale cumulus parameterization scheme operating within a global spectral model. We

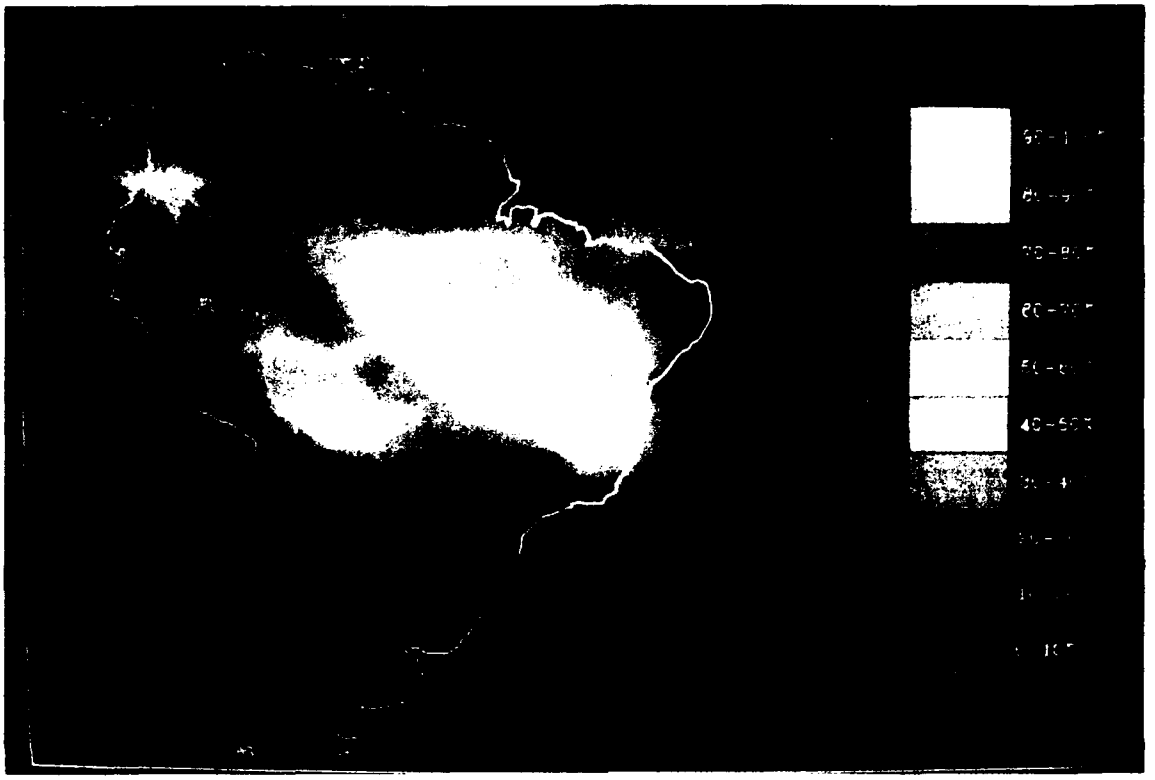

FIG. 5. Average model-generated percent total cumulus coverage during the period 29 January–14 February 1979 for model grid boxes.

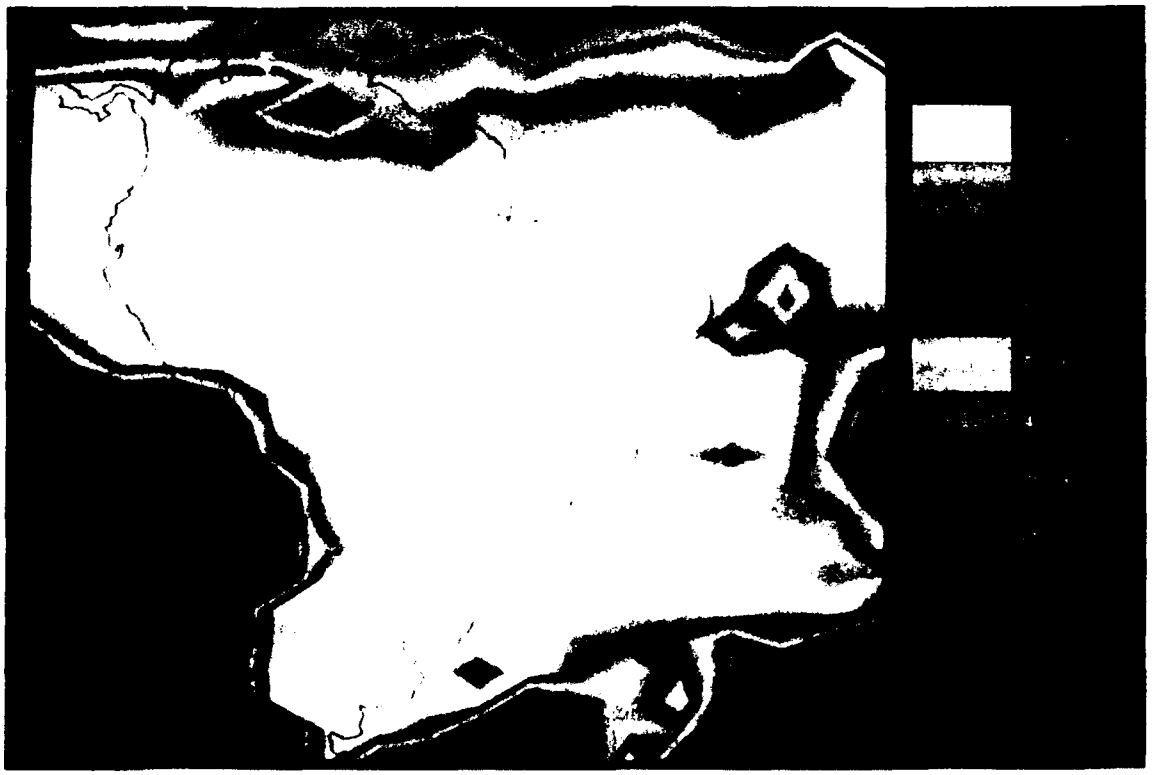

FIG. 6. High-cloud coverage as a percentage of average model-generated total cumulus coverage during the period 29 January–14 February 1979 for model grid boxes.

FIG. 7. Average satellite-observed percent total cloud coverage during the period 30 January–15 February 1979 for 250 × 250-km^2 areas.

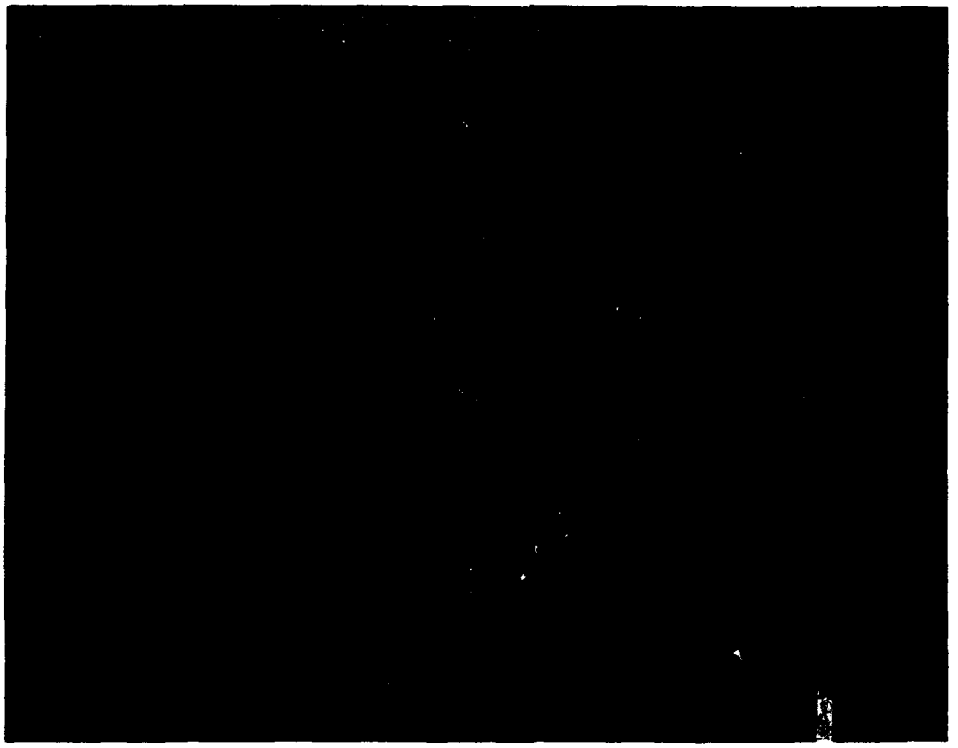

FIG. 8. High-cloud coverage as a percentage of average satellite-observed total cloud coverage during the period 30 January–15 February 1979 for 250 × 250-km^2 areas.

FIG. 9. Diurnal range of model-generated high-cloud cover (%) during the period 29 January–14 February 1979 for model grid boxes.

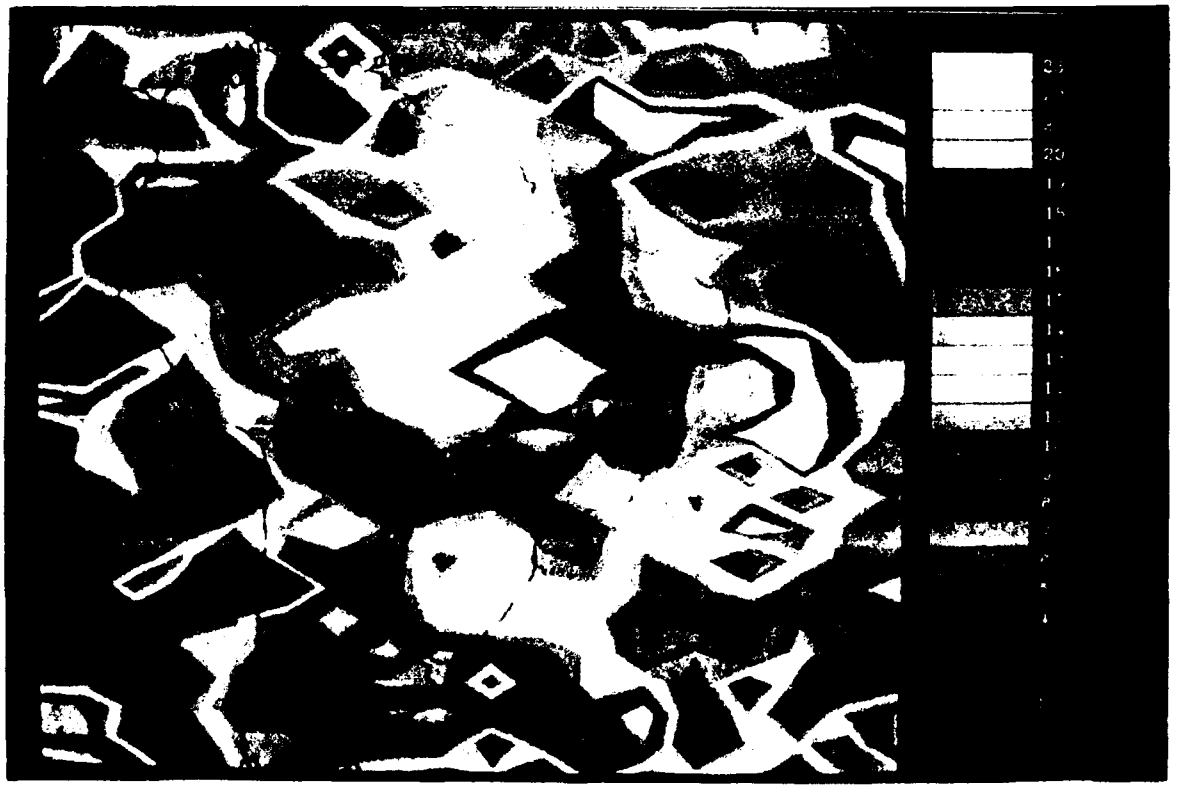

FIG. 10. Local time of maximum model-generated total cloud cover during the period 29 January–14 February 1979 for model grid boxes.

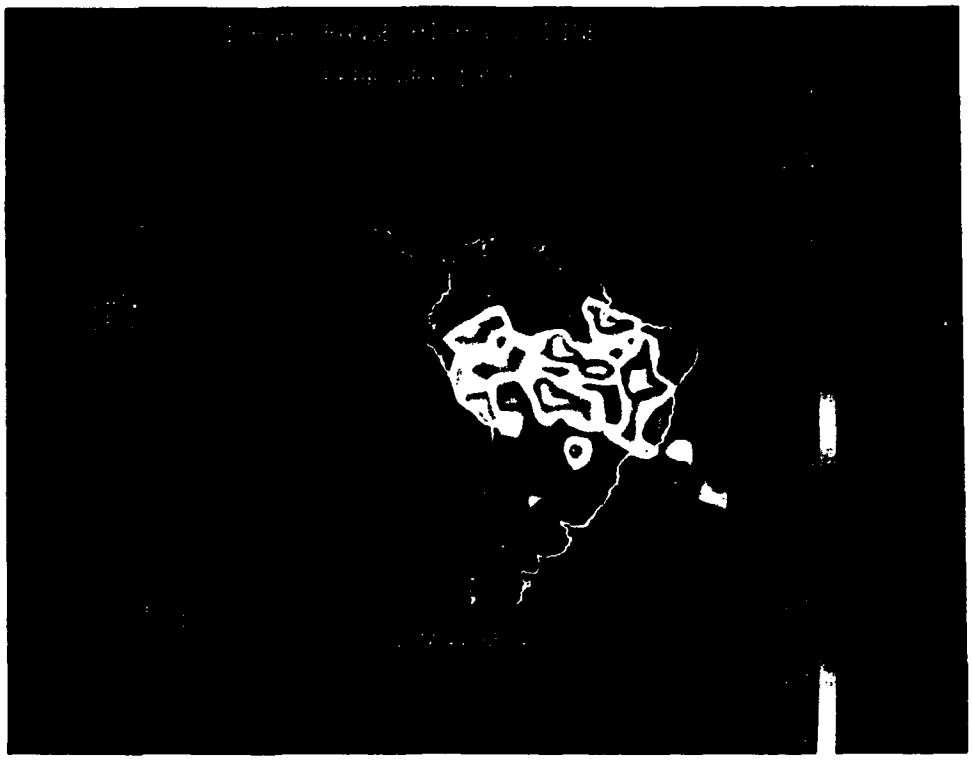

FIG. 11. Diurnal range of satellite-observed high-cloud cover (%) during the period 30 January–15 February 1979 for 250 × 250-km² areas.

compared model-generated cumulus cloud coverage within model grid boxes with analyses of observed cloudiness from geosynchronous satellite infrared data. The investigation was carried out over a section of the equatorial Pacific Ocean in January–February 1979 and over the Amazon basin in February 1979. The goal of this study was to demonstrate that geosynchronous satellite-observed cloudiness is a useful tool in verifying the spatial and temporal distribution of the intensity of model-generated cumulus convection.

The particular cumulus scheme used in this study is the Kuo (1974) convection parameterization scheme with the Krishnamurti et al. (1976) closure in the PL GSM. It overdevelops cumulus in vertical extent as compared with satellite observations. This means that, in general, too much of the heating of the large-scale tropical atmosphere occurs in the upper troposphere, leaving a deficit of heating of the lower troposphere. Yang et al. (1990) have documented a similar problem in the NMC MRF model, noting too much tropical high cloudiness. They pointed to a lack of entrainment in its convective scheme as a possible cause.

We did attempt to address the issue of the excessive vertical extent of the model-generated cumulus in a separate experiment. We derived an empirical relationship between the moisture-partitioning parameter (from Krishnamurti et al. 1976) and the cloud-top pressure that would force the vertical distribution of cumulus in the equatorial Pacific to fit that of Albright et al. (1985). This was done by mapping the approximate cumulative percentage of cloud achieving increasingly higher pressure-level thresholds (lower altitudes) onto the cumulative percentage of occurrence of heating-partitioning parameter (complement of moisture-partitioning parameter) categories in this region. This type of mapping of cumulative frequencies of occurrence is analogous to that used by Mitchell and Hahn (1990) to derive cloud-relative humidity relationships. The result was a relationship between values of heating-partitioning parameter and corresponding pressure-level cumulus-top thresholds. The limiting cloud-top pressure decreases with increasing heating partitioning parameter value. It was found, for example, that a heating fraction of 0.9 (90% of moisture supply going to condensation) would limit cloud top to a pressure level not less than 27 kPa. Heating fraction values of 1.0 (occurring about 32% of the time) will ensure convection ascending fully to the level of zero buoyancy without a limiting threshold. Applying the Kuo (1974) entrainment formulation in the manner of Soong et al. (1985) at these distinct imposed cloud-top limits resulted in a vertical distribution of model-generated cumulus as depicted in Fig. 12. The cloud coverage is slightly reduced at −18°C, somewhat more reduced at −36°C, and appreciably reduced at −55°C from the corresponding fields depicted in Fig. 1. Inclu-

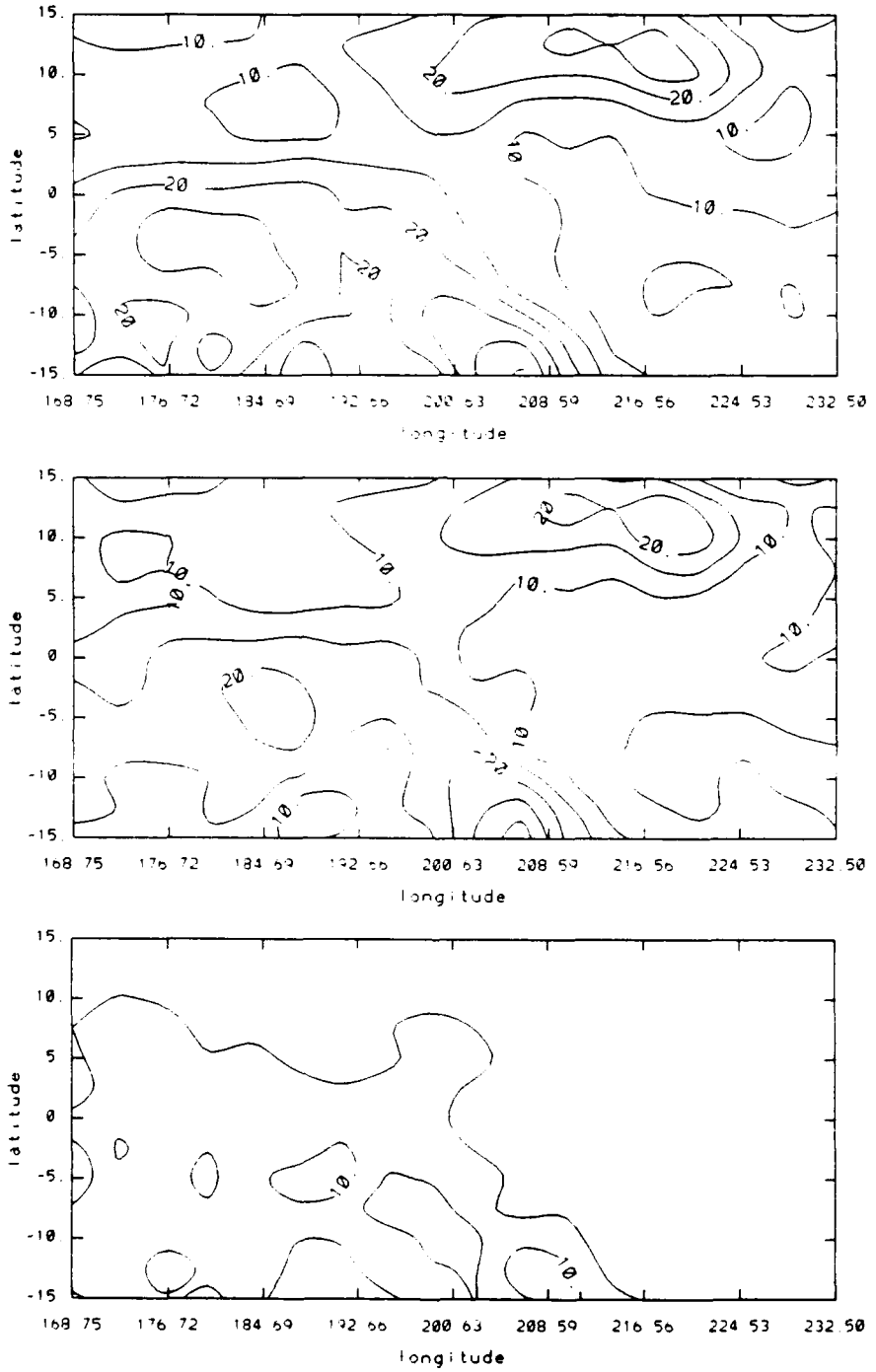

FIG. 12. Average model-generated percent cumulus coverage (using the empirical entrainment formulation) during the period 13 January–6 February 1979 for model grid boxes by clouds with tops colder than (a) −18°C, (b) −36°C, (c) −55°C.

sion of entrainment in the scheme appears to lend some control to the vertical development of cumulus. However, this type of approach is highly empirical. The cloud-top pressure–cumulus-heating parameter relationship would probably vary significantly in time and space. It was carried out in this study merely to help explain the cause of vertical overdevelopment of cumulus in the baseline parameterization scheme.

The model produced the most intense convection generally in the correct locations. We saw good agreement between the position of the SPCZ and the ITCZ as depicted by observed cloudiness and the zones of most intense model-generated cloudiness. The position of greatest total cloud cover as observed by satellite covered the same area within the Amazon basin region as for cloudiness produced by the model. This was further confirmed by independent analysis of satellite-observed outgoing longwave radiation, with minima (indicating coldest cloud) located squarely over the Amazon basin. Our conclusion is that the model does a good job of geographically positioning the areas of most intense moist convection. We reached the same conclusion in a separate study of the PL GSM over other tropical regions (Norquist and Yang 1990).

Calculating separate averages of observed total cloudiness and model-generated convective cloudiness at several times throughout the day allows a qualitative comparison of the diurnal variation of cloudiness. In the equatorial Pacific region, we computed the departure of the average for each of the eight UTC times of the day from the daily mean and compared these with the corresponding observed departures from Albright et al. (1985). In the Amazon basin region, we followed the procedure of Minnis and Harrison (1983) by computing an average for each hour of the day for the model-produced cumulus cloud coverages. The diurnal range is defined as the difference between the hourly maximum and minimum values.

We conclude from these comparisons of diurnal variation that the model's diurnal pattern is much more realistic over land than over oceans. Over oceans, the model seems to be 9–12 h out of phase with the observations in prediction of maximum and minimum cloudiness, and the amplitudes seem to be somewhat smaller. Over land, model-produced maximum cloudiness occurs on average just 1 or 2 h earlier in the afternoon than observed. The high-cloud diurnal variations agree well over land. This more favorable model behavior over land may have been expected because the physical mechanisms for causation of diurnal convection patterns are much better understood over land areas (see the review of this topic in Albright et al. 1985).

Unfortunately, the limitations of this study do not allow a quantitative comparison between model-generated and observed cloudiness. This is primarily because satellites observe all forms of cloud, and from the infrared sensor estimates of cloud-top temperature, only an approximate altitude position can be assigned. In this study, on the other hand, the model cloud amount is diagnosed from the precipitation rate using an empirical relationship based on observed tropical convective cloudiness and model precipitation rates. Hence, we can only compare cloudiness qualitatively and only in areas known to be dominated by convective cloud. Still, this allows comparison to be conducted in most of the regions where the convection scheme would be expected to have its greatest effect on the model atmosphere.

In this study we chose to use the results of other investigators' analyses of satellite data and to compare model-generated cloudiness to them. A disadvantage of this approach is that the model has to be run for the time and place of the satellite observations. Strictly speaking, this limits the applicability of the comparison to just that time and region. We expect, however, that our conclusions may be generally valid over all areas of intense tropical convection, but cannot prove this without comparisons conducted in other times and regions (for example, over the East Indies or central Africa in June).

A benefit of using pure observations or analyses based solely on observations (such as those used here) as a reference, rather than a hybrid of a model and observations (such as in a standard analysis of large-scale meteorological fields), is that the results are not biased toward any one model. Entirely different conclusions about the efficacy of cumulus parameterization may be drawn from any two schemes. The geosynchronous satellite–observed cloudiness data is a reference that is not limited in its applicability to a single convection scheme or model.

The vertical extent of the model-generated convective cloud depends on the value of equivalent potential temperature, which defines the moist adiabat, and on the environmental temperature profile at the same grid location. The equivalent potential temperature in turn depends on the temperature and water vapor mixing ratio near the surface (the base level for the parcel of air). It is obvious that the vertical penetration of parameterized cloudiness in such a scheme depends on the model temperature and moisture forecasts at each step. Cumulus parameterization is only one component in determining these forecast values. Other model components such as the hydrodynamics and other physical parameterization packages also play a major role. For this reason, it is not possible to apply conclusions from this type of study to a similar convective parameterization scheme operating within a different forecast model. Yet the comparison procedure used in this study can be readily repeated for any large-scale model, and as such, provides a useful tool in assessing the validity of such a model.

Acknowledgments. We wish to express our appreciation to Mark Albright and Patrick Minnis for supplying us with the figures from their respective papers. Douglas Hahn provided invaluable help in producing the color graphics of the model-generated cloud fields. Audrey Campana and Anna Tortorici performed the word processing task. This research was supported by the Air Force Office of Scientific Research.

REFERENCES

Albright, M. D., E. E. Recker, R. J. Reed, and R. Dang, 1985: The diurnal variation of deep convection and inferred precipitation in the central Pacific during January–February 1979. *Mon. Wea. Rev.*, **113**, 1663–1680.

Arkin, P. A., and B. N. Meisner, 1987: The relationship between large-scale convective rainfall and cold cloud over the western hemisphere during 1982–84. *Mon. Wea. Rev.*, **115**, 51–74.

Bess, T. D., and G. L. Smith, 1987: *Atlas of Wide-Field of View Outgoing Longwave Radiation Derived from Nimbus 7 Earth Radiation Budget Data Set—November 1978 to October 1985*. NASA Reference Publication 1186, NASA Langley Research Center, Hampton, VA.

Grell, G., Y.-H. Kuo, and R. Pasch, 1988: Semi-prognostic tests of three cumulus parameterization schemes for mid-latitude convective systems. Preprints, *Eighth Conf. on Numerical Weather Prediction*, Baltimore, Amer. Meteor. Soc.

Kanamitsu, M., 1989: Description of the NMC global data assimilation and forecast system. *Wea. Forecasting*, **4**, 335–342.

Krishnamurti, T. N., M. Kanamitsu, R. Godbole, C.-B. Chang, F. Carr, and J. H. Chow, 1976: Study of a monsoon depression (II), dynamical structure. *J. Meteor. Soc. Japan*, **54**, 208–225.

Kuo, H.-L., 1974: Further studies of parameterization of the influence of cumulus convection on large-scale flow. *J. Atmos. Sci.*, **31**, 1232–1240.

Leary, C. A., and R. A. Houze Jr., 1980: The contribution of mesoscale motions to the mass and heat fluxes of an intense tropical convective system. *J. Atmos. Sci.*, **37**, 784–796.

Liou, K.-N., S.-C. Ou, S. Kinne, and G. Koenig, 1984: *Radiation Parameterization Programs for Use in General Circulation Models*. AFGL-TR-84-0217, Air Force Geophysics Laboratory, Hanscom AFB, MA. [NTIS ADA 148015.]

Lord, S. J., 1982: Interaction of a cumulus cloud ensemble with the large-scale environment. Part III: Semi-prognostic test of the Arakawa-Schubert cumulus parameterization. *J. Atmos. Sci.*, **39**, 88–103.

Louis, J.-F., R. N. Hoffman, T. Nehrkorn, and D. Norquist, 1989: Observing system experiments using the AFGL four-dimensional data assimilation system. *Mon. Wea. Rev.*, **117**, 2186–2203.

Mahrt, L., H.-L. Pan, P. Ruscher, and C.-T. Chu, 1987: *Boundary Layer Parameterization for a Global Spectral Model*. AFGL-TR-87-0246, Air Force Geophysics Laboratory, Hanscom AFB, MA. [NTIS ADA 199440.]

Miller, B. L., and D. G. Vincent, 1987: Convective heating and precipitation estimates for the tropical South Pacific during FGGE, 10–18 January 1979. *Quart. J. Roy. Meteor. Soc*, **113**, 189–212.

Minnis, P., and E. F. Harrison, 1983: Diurnal and seasonal variations of clouds from geostationary satellite data. Preprints, *Fifth Conf. on Atmospheric Radiation*, Baltimore, Amer. Meteor. Soc.

Mitchell, K. E., and D. C. Hahn, 1990: Objective development of diagnostic cloud forecast schemes in global and regional models. Preprints, *Seventh Conf. on Atmospheric Radiation*, San Francisco, Amer. Meteor. Soc., J138–J145.

Norquist, D. C., and C.-H. Yang, 1990: *Refinement and Testing of the Moist Convection Parameterization in the GL Global Spectral Model*. GL-TR-90-0285, Geophysics Laboratory (AFSC) Hanscom AFB, MA. [Available from PL/GPAP, Hanscom AFB, MA 01731.]

Slingo, J. M., 1987: The development and verification of a cloud prediction scheme for the ECMWF model. *Quart. J. Roy. Meteor. Soc.*, **113**, 899–927.

Soong, S-T., Y. Ogura, and W.-S. Kau, 1985: *A Study of Cumulus Parameterization in a Global Circulation Model*. AFGL-TR-85-0160, Air Force Geophysics Laboratory, Hanscom AFB, MA. [NTIS ADA 170137.]

Yanai, M., S. K. Esbensen, and H. H. Chu, 1973: Determination of bulk properties of tropical cloud clusters from large-scale heat and moisture budgets. *J. Atmos. Sci.*, **30**, 611–627.

Yang, S. K., H. M. Juang, K. A. Campana, and A. J. Miller, 1990: Validating cloud field and outgoing longwave radiation generated by NMC medium range forecast model with ERBE and Air Force real time nephanalysis. Preprints, *Seventh Conf. on Atmospheric Radiation*, San Francisco, Amer. Meteor. Soc., 145–148.

DTIC QUALITY INSPECTED 1

Accession For
NTIS GRA&I ☑
DTIC TAB ☐
Unannounced ☐
Justification
By
Distribution/
Availability Codes
Dist | Avail and/or Special
A-1 | 20